JACS
JOURNAL OF THE AMERICAN CHEMICAL SOCIETY

ARTICLE

pubs.acs.org/JACS

Magnetism of Phthalocyanine-Based Organometallic Single Porous Sheet

Jian Zhou[†] and Qiang Sun[*,†,‡]

[†]Department of Advanced Materials and Nanotechnology, College of Engineering, Peking University, Beijing 100871, China
[‡]Center for Applied Physics and Technology, Peking University, Beijing 100871, China

Supporting Information

ABSTRACT: A two-dimensional (2D) periodic Fe phthalocyanine (FePc) single-layer sheet has very recently been synthesized experimentally (Abel, M.; et al. *J. Am. Chem. Soc.* **2011**, *133*, 1203), providing a novel pathway for achieving 2D atomic sheets with regularly and separately distributed transition-metal atoms for unprecedented applications. Here we present first-principles calculations based on density functional theory to investigate systematically the electronic and magnetic properties of such novel organometallics (labeled as TMPc, TM = Cr−Zn) as free-standing sheets. Among them, we found that only the 2D MnPc framework is ferromagnetic, while 2D CrPc, FePc, CoPc, and CuPc are antiferromagnetic and 2D NiPc and ZnPc are nonmagnetic. The difference in magnetic couplings for the studied systems is related to the different orbital interactions. Only MnPc displays metallic d_{xz} and d_{yz} orbitals that can hybridize with p electrons of Pc, which mediates the long-range ferromagnetic coupling. Monte Carlo simulations based on the Ising model suggest that the Curie temperature (T_C) of the 2D MnPc framework is ∼150 K, which is comparable to the highest T_C achieved experimentally, that of Mn-doped GaAs. The present study provides theoretical insight leading to a better understanding of novel phthalocyanine-based 2D structures beyond graphene and BN sheets.

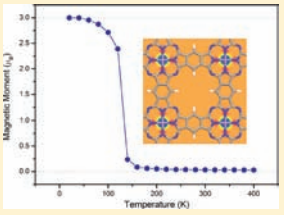

I. INTRODUCTION

Tremendous effort is currently being devoted to two-dimensional (2D) atomic sheet-based materials. The existing systems include graphene sheets[1] and BN sheets.[2] Manipulating the geometric and electronic structures of these 2D atomic sheets for practical applications has been an important and challenging topic in this field. Patternization with regular pores in a graphene sheet has successfully been achieved,[3] which not only can open the energy band gap but also provides unprecedented possibilities for introducing atoms, molecules, and functional groups to the regular pores for further functionalization. However, for metal atoms, especially transition-metal (TM) atoms, preventing the introduced atoms from clustering is extremely challenging because of the strong d−d interactions. At present, no research on the regular docking of TM atoms onto the pores in graphene sheets has been reported. The recent success in embedding TM atoms in 2D phthalocyanine (Pc) sheets provides a novel pathway for achieving the long-standing dream of 2D atomic sheets with regularly and separately distributed TM atoms for catalysis, hydrogen storage, and spintronics. For example, Abel et al.[4] successfully achieved polymerization of FePc molecules directly. They synthesized a single-layer 2D periodic FePc framework through a metal-directed surface reaction, and the samples were characterized using scanning tunneling microscopy (STM) at room temperature. They also pointed out that the synthesis procedure is flexible for other central metal atoms. It can be expected that other TM-based 2D Pc sheets can be synthesized in the future. For further development and applications, a systematic understanding of these sheets would be highly desirable. Although the electronic and magnetic properties of *monomeric* TMPc *molecules* and their stacking structures have been studied,[5−23] the knowledge about the basic magnetic properties and intrinsic couplings of such novel TM-based 2D frameworks is still lacking.

In the present study, using first-principles calculations combined with Monte Carlo (MC) simulations, we systematically investigated the magnetic behaviors of free-standing 2D TMPc sheets, which is the first step in understanding sheets deposited on diverse substrates. We chose TM atoms ranging from Cr to Zn in the periodic table and focused on the magnetic coupling of the 2D sheets and the magnetic behaviors of the ferromagnetic systems at different temperatures. We show that except for TM = Ni and Zn, which have nonmagnetic (NM) ground states, the other TMPc frameworks are magnetic. Further magnetic-coupling calculations showed that for TM = Mn, the framework is ferromagnetic (FM), while for TM = Cr, Fe, Co, and Cu, the coupling is antiferromagnetic (AF). The magnetic moments of Cr−Zn are approximately 4, 3, 2, 1, 0, 1, and 0 μ_B, respectively. Moreover, for the FM 2D MnPc system, we further estimated the Curie temperature (T_C) using mean-field theory (MFT) as well as MC simulations based on the Ising model, and we found the possibility of long-ranged cooperative magnetic order near room temperature.

II. COMPUTATIONAL PROCEDURES

Our first-principles calculations were based on spin-polarized density functional theory (DFT) using the generalized gradient approximation

Received: June 4, 2011
Published: August 13, 2011

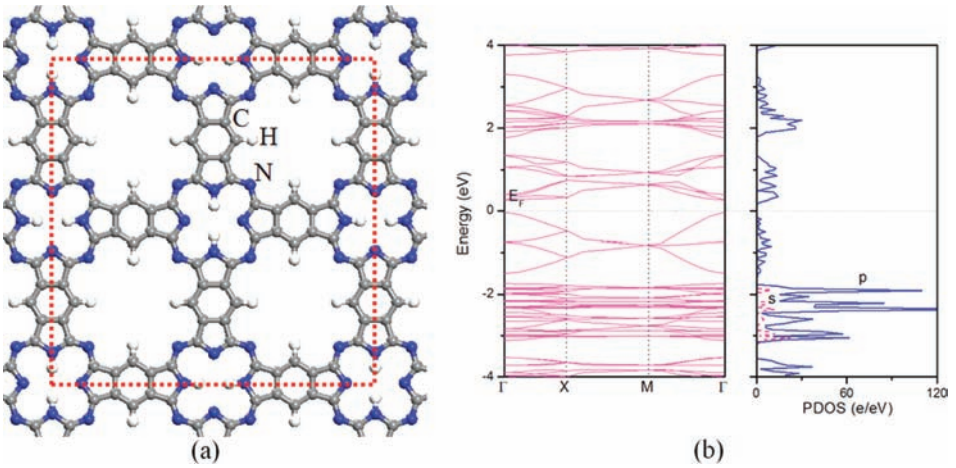

Figure 1. (a) Geometric structure and (b) band structure and corresponding PDOS of the 2D Pc framework. The dashed rectangle in (a) denotes the supercell. Γ (0, 0, 0), X (0, $^1/_2$, 0), and M ($^1/_2$, $^1/_2$, 0) are highly symmetric points in reciprocal space.

(GGA)[24] in the form proposed by Perdew, Burke, and Ernzerhof (PBE) as implemented in the Vienna ab initio simulation package (VASP) code.[25] Because the GGA cannot properly describe strongly correlated systems containing partially filled d subshells, we used the GGA+U method[26] by dividing the electrons into two classes: delocalized s and p electrons, which can be well-described by the GGA, and the localized d electrons, which are described by Coulomb and exchange corrections. In this way, we were able to obtain a qualitative improvement not only for excited-state properties such as energy gaps but also for ground-state properties such as magnetic moments and interatomic exchange parameters. We used a correlation energy (U) of 4 eV and an exchange energy (J) of 1 eV for TM d orbitals; these values have been tested and used in previous experimental and theoretical works.[27−32] We also tested U = 6 eV for the CoPc framework proposed in ref 11 and obtained results quite similar to those for U = 4 eV. The projected augmented wave (PAW) method[33,34] with a plane-wave basis set was used. For the spin-polarized calculations, the Vosko−Wilk−Nusair modification[35] scheme was applied to interpolate the correlation energy. The valence electron configurations for TM = Mn−Ni and Zn were $3d^n4s^2$ with n = 5−8 and 10, respectively; for Cr and Cu, the configurations were $3d^54s^1$ and $3d^{10}4s^1$, respectively. We applied periodic boundary conditions and a vacuum space of 15 Å along the z direction in order to avoid interactions between two TMPc images in nearest-neighbor unit cells. All of the structures were relaxed using the conjugated gradient method without any symmetric constraints. To investigate the magnetic coupling between the TM atoms, we performed the calculations using a (2 × 2) supercell. The Monkhorst−Pack special **k**-point meshes[36] of 9 × 9 × 1 and 5 × 5 × 1 were used for the unit cell and the (2 × 2) supercell, respectively, to represent their reciprocal spaces. We set the energy cutoff and convergence criteria for energy and force to be 400 eV, 1×10^{-4} eV, and 0.01 eV/Å, respectively. The accuracy of our simulation procedure was tested through a comparison of the calculated lattice constant (10.70 Å) and the experimental value (1.15 ± 0.1 nm) for the 2D FePc framework, which showed good agreement.[4] In addition, the geometric structures and total magnetic moments of the TMPc molecules were calculated and found to be consistent with previous theoretical results.[7,11]

III. RESULTS AND DISCUSSION

Before examining 2D TMPc sheets, we first studied the geometric and electronic properties of the metal-free 2D Pc framework, as shown in Figure 1. Structural relaxation suggests that such a framework is planar without any buckling, similar to pristine graphene and BN sheets. The supercell lattice constant (dashed rectangle in Figure 1a) was optimized to be 21.51 Å. We found that this π-conjugated system is a nonmagnetic semiconductor with a calculated band gap of 0.29 eV (Figure 1b). Although the GGA underestimates the energy band gap, this calculated band gap is much smaller than the gaps calculated at a similar theoretical level for conventional semiconductors such as Si, GaAs, and ZnO, thus providing the feasibility of band engineering for potential applications. Furthermore, we found that both the valence band maximum (VBM) and conduction band minimum (CBM) are located at the Γ point of the reciprocal space, indicating a direct band gap in the system. The partial density of states (PDOS) clearly shows that p electrons play dominant roles in the bonding.

When TM atoms are introduced into the Pc pores, 2D porous structures with *regularly separated* 3d TM atoms are formed. The geometric structures of 2D TMPc are shown in Figure 2. Such structures would exhibit some interesting magnetic properties in comparison with dilute magnetic semiconductors (DMSs) such as Mn-doped Si, GaN, or ZnO, where the doped TM atoms easily form clusters,[37,38] thus resulting in nonintrinsic magnetism and low T_C values.

It is known that in a square-planar-coordinated crystal-field environment, the d bands split into four bands: a doubly degenerate d_π band (d_{xz} and d_{yz}) and singly degenerate d_{z^2}, d_{xy}, and $d_{x^2-y^2}$ bands. Thus, as the d bands are sequentially filled from Cr to Zn, when one of the degenerate d bands is partially filled, Jahn−Teller distortions should occur in order to remove the degeneracy and lower the energy. We found that when standard GGA without the U correlation was applied, no Jahn−Teller distortions were observed for any of the systems. However, when GGA+U was used, we did find the Jahn−Teller distortions, causing in-plane shifts for Mn and Co. The bond lengths between the central TM atoms and the host N atoms in all of the structures are shown in Table 1, where we can see that the TM−N distance decreases in going from CrPc (2.001 Å) to CoPc (1.917 Å on average) and then increases until ZnPc (1.994 Å). This trend is consistent with the variations of the radii of the four-coordinate TM atoms in their +2 valence states,[39] where two electrons of each TM atom form the bonding with the host Pc framework. All of the geometrical coordinates are presented in the Supporting Information.

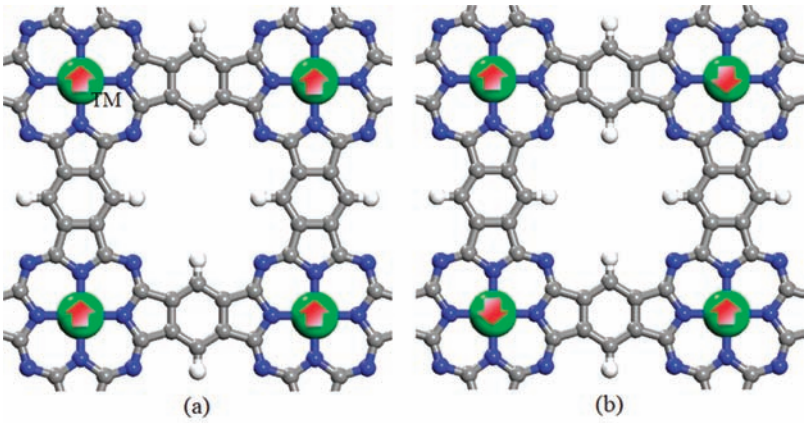

Figure 2. Illustrations of (a) ferromagnetic and (b) antiferromagnetic coupling between the central TM atoms. Arrows indicate spin directions of the central TM atoms.

Table 1. Bond Lengths between the Central TM Atoms and the Neighboring N Atoms (d_{TM-N}, in Å), Exchange Energies per Supercell (E_{ex}, in meV), Total Magnetic Moments per Unit Cell (M, in μ_B), and Energy Band Gaps (E_g, in eV) for 2D TMPc Frameworks

	Cr	Mn	Fe	Co	Ni	Cu	Zn
d_{TM-N}[a]	2.001	1.958	1.957	1.912	1.922	1.964	1.994
		1.962		1.921			
E_{ex}	−29	124	−14	−6	–	−7	–
M	4	3	2	1	0	1	0
E_g	0.36	half-metal	0.24	0.10	0.34	0.31	0.30

[a] For Mn and Co, two values are given because there are two TM−N distances as a result of in-plane shifts of the TM atoms.

To study the preferred magnetic coupling, the energies of the FM and AF states of the (2 × 2) supercell for each TM were calculated (Figure 2; detailed numerical results are given in the Supporting Information). The exchange energy E_{ex} (= $E_{AF} - E_{FM}$) per supercell and the total magnetic moment M of each unit cell are listed in Table 1. A positive (negative) exchange energy indicates that the ground state of the system is FM (AF). It was found that FM coupling exists only in 2D MnPc with E_{ex} = 124 meV per (2 × 2) supercell (i.e., 15.5 meV exchange energy for each two nearest-neighbor Mn atoms). On the other hand, the couplings in 2D CrPc, FePc, CoPc, and CuPc are all AF with small exchange energies, and 2D NiPc and ZnPc show no magnetism. For 2D CoPc, we also used U = 6 eV[11] to calculate E_{ex} and obtained a value of −2 meV. This value is comparable to the value of −6 meV for U = 4 eV within the precision of the DFT calculations, suggesting the reliability of the U and J values we used in the calculations. For the magnetic frameworks, our calculations showed that the central metal atoms carry most of the magnetic moment in the unit cell while their nearest-neighbor N atoms are polarized antiferromagnetically, except for CuPc, which has ferromagnetic polarizations at N sites. Other C, N, and H atoms in the host Pc are slightly spin-polarized. We should point out that the standard GGA also yielded the same trend qualitatively. The isosurface and a 2D slice of the spin density ($\rho_\uparrow - \rho_\downarrow$) for FM 2D MnPc is illustrated in Figure 3a, showing the polarization of Pc substrate.

In order to understand the electronic and magnetic structures of all these systems, we analyzed the projected density of states of the d electrons of the central metal atoms in the ground states (Figure 3c and 4). Since the s electrons of the central metal atoms form bonds with the host Pc, only 3d electrons participate in orbital splitting in the square-planar crystal field and contribute to the magnetism. In the 2D CrPc framework, we find that the d_π, d_{z^2}, and d_{xy} orbitals of Cr are occupied by four spin-up electrons, where the two d_π orbitals are energetically degenerate and thus hybridized, forming wider bands than the others (Figure 4a). All of the other bands are unoccupied, resulting in a magnetic moment of 4 μ_B for each unit cell of the CrPc framework. Moreover, the introduction of Cr enhances the energy gap to ∼0.36 eV.

The situation is changed when Mn instead of Cr is introduced. In this case, because of the strong hybridization with the ligand π bands, the spin-down d_π bands are broadened and shifted upward in energy to lie above the spin-down d_{xy} and d_{z^2} orbitals. When one electron is inserted into the spin-down channel and partially occupies the d_π bands, a small Jahn−Teller distortion is induced to remove the degeneracy and lower the energy. We identified the distortion to be a planar shift of Mn, resulting in two nonequivalent Mn−N bond lengths of 1.958 and 1.962 Å, as shown in Table 1. The filling of the spin-down band reduces the magnetic moment to 3 μ_B. Furthermore, a metallic feature in the spin-down channel is induced, while the spin-up channel remains semiconducting. The band structure of 2D MnPc (Figure 3b) shows semiconducting behavior of the spin-up electrons (band gap of 0.32 eV) and metallicity of the spin-down electrons. Detailed analyses suggest that both the valence band and the conduction band in the spin-up channel arise mainly from contributions from the C and N 2p electrons of the host Pc framework, which are delocalized because they are highly dispersed. The metallic states in the spin-down channel indicate that the main contribution to the flatter band (localized) is from the 3d orbitals of the Mn atoms. The PDOS of 2D MnPc (Figure 3b right) illustrates both the p and d bands across the Fermi level. Although d electrons are generally localized, similar conductive d bands of Mn have also been observed in other systems.[40,41] Hence, the 2D MnPc framework is half-metallic with 100% spin polarization around the Fermi level, where the spin-down electrons can be freely transported through the linked benzene and pyrrole with the help of the hybridization of p and d orbitals.

For 2D FePc, the occupied spin-down states are d_{xy} and d_{z^2}, while the spin-down d_π bands are unfilled (Figure 4b), giving a

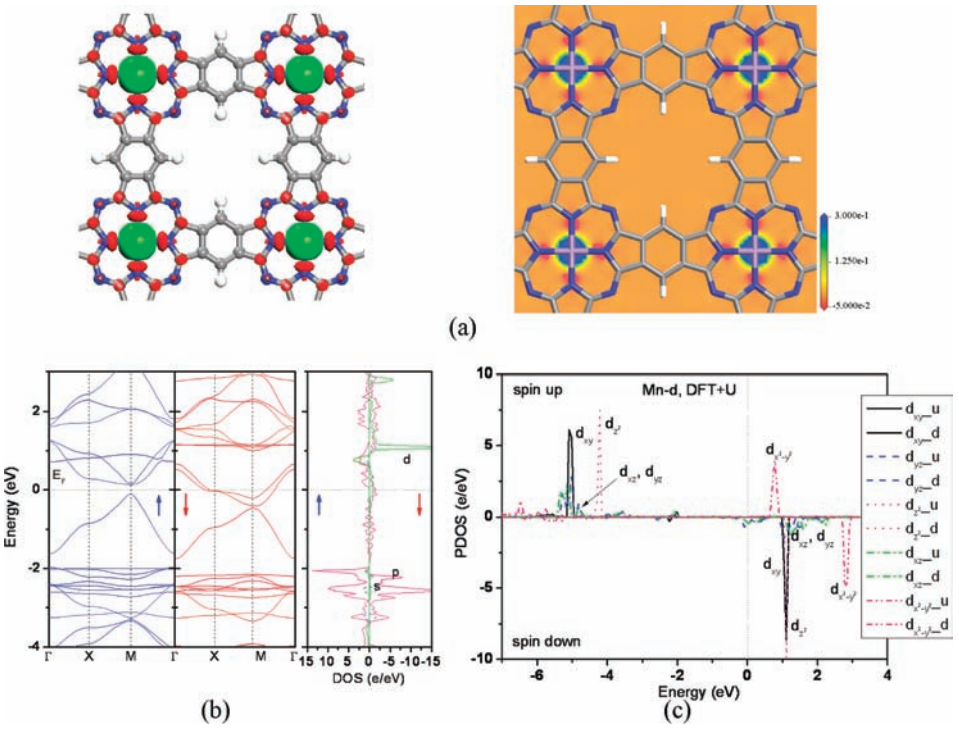

Figure 3. (a) (left) Isosurface at a value of 0.01 e/Å^3 and (right) 2D slice of the spin density ($\rho_\uparrow - \rho_\downarrow$) for FM 2D MnPc. (b) Band structure and corresponding DOS of FM 2D MnPc. (c) Projected DOS of the d orbitals on the Mn atom. Symbols: solid for d_{xy}; dash for d_{yz}; dot for d_{z^2}; dash-dot for d_{xz}; dash-dot-dot for $d_{x^2-y^2}$.

magnetic moment of 2 μ_B per unit cell. Thus, no Jahn−Teller distortions exist. For 2D CoPc, we observe that the spin-down d_{xy}, d_{z^2}, and d_{xz} are occupied, leaving d_{yz} empty (Figure 4c) and giving a magnetic moment of 1 μ_B per unit cell. This d_π band splitting is consistent with Jahn−Teller distortion of 2D CoPc (Table 1). For 2D NiPc, all of the d bands except $d_{x^2-y^2}$ are fully occupied (Figure 4d), making the system nonmagnetic. After that, the $d_{x^2-y^2}$ band is occupied by one spin-up electron in 2D CuPc (Figure 4e) and fully occupied in 2D ZnPc (Figure 4f).

Among the magnetic frameworks, only the MnPc system is ferromagnetic with a large exchange energy. This can be understood by checking the electronic structures as shown in the PDOS in Figure 3c, where the conductive d bands provide channels for effective coupling via d−p exchange with the host Pc. In contrast, the d bands in the other structures exhibit gaps, as shown in Figure 4. The existing band gaps make the d−p exchange less effective and result in AF or NM states for these systems.

The calculated energy band gaps are listed in Table 1. Our test calculations on an isolated NiPc molecule yielded an energy gap of 1.46 eV, which agrees well with the previously reported value (1.47 eV)[7] and is much larger than that for the 2D NiPc sheet (0.34 eV). This result suggests that strong orbital hybridizations in the assembled 2D sheet reduce the energy band gap, similar to what happens in going from benzene molecules to a graphene sheet. Among the studied systems, we found that 2D CoPc exhibits the smallest band gap (0.10 eV) as a result of the d_π splitting; the gap for 2D FePc (0.24 eV) is slightly smaller than that for the metal-free Pc framework (0.29 eV), while others have band gaps of ≥0.30 eV. These results indicate that the central TM atoms have limited influences on the band gaps of the 2D TMPc structures, which is a consequence of the fact that the main contributions to the valence and conduction bands are from the p orbitals of the host Pc.

Above we have seen that among all of the studied systems, only the 2D MnPc sheet shows ferromagnetism. For future applications such as in spintronic devices, we need to get a more in-depth understanding especially of the changes in magnetism with temperature. To this end, we used Ising model, in which the Hamiltonian can be written as $\hat{H} = -\sum_{i,j} J' \hat{\mathbf{m}}_i \cdot \hat{\mathbf{m}}_j$, where $\mathbf{m}_i$ and $\mathbf{m}_j$ are the magnetic moments at sites i and j and J' is the exchange parameter. The value of J' is determined from the exchange energy E_{ex} by the relation $J' = (^1/_8)E_{ex}/2m^2$, where $m = |\mathbf{m}|$ and the factor of $^1/_8$ is included because there are altogether eight magnetic coupling interactions in one (2×2) supercell. Hence, we estimated the exchange parameter J' to be 0.86 meV. With the help of these parameters, we applied the MFT to estimate the magnetic properties of 2D MnPc. The partition function was first computed by considering all possible spin configurations according to the spin multiplicity of Mn, and then the Curie temperature T_C was obtained by determining the bifurcation critical point of the ensemble-average magnetic moment $\langle m \rangle$. The details are stated as follows. The partition function can be written as

$$Z = \sum_{m=3,1,-1,-3} e^{\gamma J' m \langle m \rangle / k_B T} = 2\cosh\frac{\gamma J' \langle m \rangle}{k_B T} + 2\cosh\frac{3\gamma J' \langle m \rangle}{k_B T} \quad (1)$$

where $\gamma = 4$ is the coordination number of the Mn atoms and the possible values of m are 3, 1, −1, and 3 because the calculated magnetic moment in the unit cell is 3 μ_B for the MnPc system.

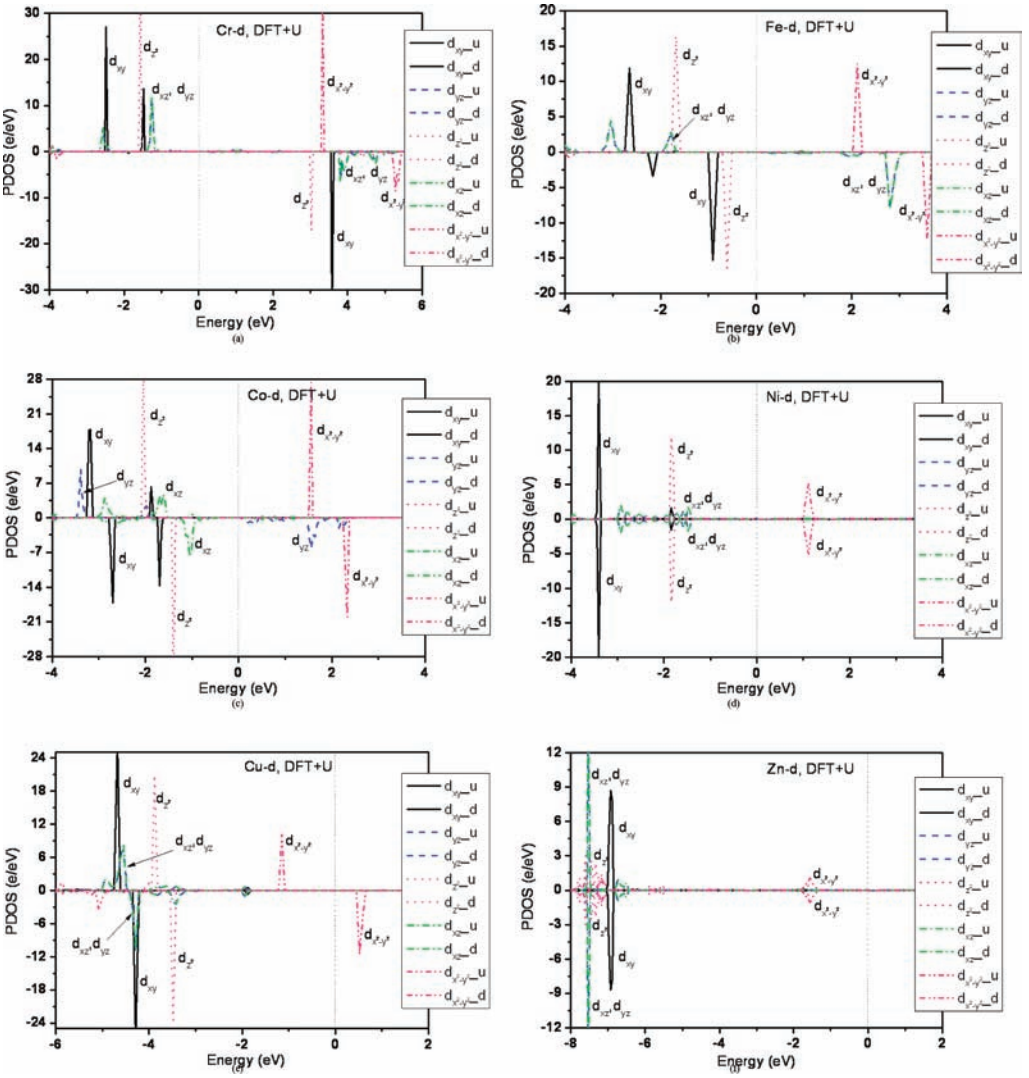

Figure 4. Projected DOS of d orbitals on the TM atom when TM is (a) Cr, (b) Fe, (c) Co, (d) Ni, (e) Cu, and (f) Zn.

Therefore, the average spin of each magnet is

$$\langle m\rangle = \frac{1}{Z}\left[2\sinh\frac{\gamma J'\langle m\rangle}{k_B T} + 6\sinh\frac{3\gamma J'\langle m\rangle}{k_B T}\right] \quad (2)$$

If p is defined as $\gamma J'/k_B T$, then the above equation can be rewritten as

$$\langle m\rangle = \frac{\sinh(p\langle m\rangle) + 3\sinh(3p\langle m\rangle)}{\cosh(p\langle m\rangle) + \cosh(3p\langle m\rangle)} \quad (3)$$

It can be easily deduced that when the parameter p changes, the static solution $\langle m\rangle$ varies, and the critical point is $p_C = \gamma J'/k_B T_C = {}^1/_5$. This corresponds to the phase transition of the system between ferromagnetic and paramagnetic states, which occurs at T_C. The value of T_C for 2D MnPc is thus obtained as ~199.8 K.

Because of the possible overestimation of T_C predicted by the MFT method, next we performed MC simulations of the magnetic moment as a function of temperature in order to obtain T_C more precisely. In the MC simulations, an (80×80) supercell was used, and the calculation lasted for 5×10^5 loops; in each loop, the spins on all the sites in the supercell changed according to the spin states of Mn. Thus, altogether 3.2×10^9 trials were performed in the simulations. We also found that using a larger supercell or longer loops had only a marginal influence on the final results. The results of the MC simulations are shown in Figure 5. It can be seen that the magnetic moment per unit cell starts dropping gradually from 3 μ_B at ~60 K, the paramagnetic state is achieved at a temperature of ~150 K for 2D MnPc, which is reduced by 25% relative to the MFT estimate discussed above. It should be noted that if a Heisenberg model is used with the inclusion of magnetic anisotropy and quantum fluctuations, the calculated Curie temperature may be different.

The value of T_C for 2D MnPc obtained from the MC simulations is quite comparable to the highest T_C achieved experimentally in Mn-doped GaAs.[28] Here we see again the unique feature of Mn-doped structures for ferromagnetism. Mn atoms, because of their special electronic configuration of $3d^5 4s^2$, have been widely used as a dopant for various semiconducting substrates such as GaAs, GaN, ZnO, AlN, and SiC, where the distributions of doped Mn atoms are highly sensitive to the synthesis process and conditions; thus, the Curie temperatures reported by different groups are quite different, and even the magnetic couplings are in conflict.[42−46] Furthermore, the conventional DMSs also suffer from the problem of low solubility of

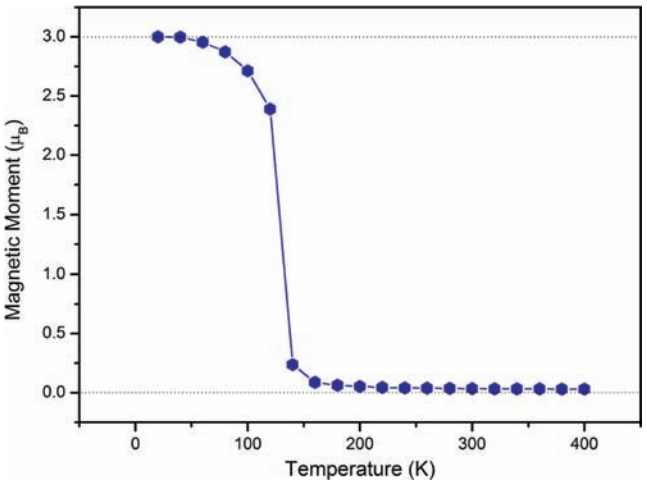

Figure 5. Variation of the total magnetic moment per unit cell of 2D MnPc with respect to the temperature.

transition metals in the substrate. Therefore, the good controllability and high concentration of Mn are additional advantages of 2D MnPc for potential applications in spintronics in comparison with traditional DMSs.

IV. SUMMARY

In summary, using DFT (GGA+U), we have systematically studied the electronic and magnetic properties of the transition-metal atoms Cr to Zn embedded in a 2D phthalocyanine framework. The following conclusions can be made: (1) The in-plane Jahn−Teller effect is identified for 2D MnPc and CoPc as a result of the square-coordinated crystal-field effect. (2) Only the 2D MnPc framework has a ferromagnetic ground state, which possesses conductive d bands in its spin-down channel for effective p−d exchange. In contrast, the other TMPc frameworks, with semiconducting d bands, have antiferromagnetic or nonmagnetic ground states. (3) By applying Monte Carlo simulations based on the Ising model, we predict that the Curie temperature of 2D MnPc is ∼150 K, which is comparable to the highest T_C value achieved experimentally for Mn-doped GaAs; the mean field theory calculation overestimates the T_C by ∼25%. (4) A 2D TMPc sheet can be a half-metal or a semiconductor, and the electronic and magnetic properties as well as the catalysis and adsorption can be tuned by embedding diverse metal atoms in controllable and feasible ways, exhibiting more flexibility and freedom than for graphene and BN sheets. We hope that the present study will stimulate further experimental effort in this field.

■ ASSOCIATED CONTENT

Supporting Information. Geometric coordinates; total energies of TMPc frameworks. This material is available free of charge via the Internet at http://pubs.acs.org.

■ AUTHOR INFORMATION

Corresponding Author
sunqiang@pku.edu.cn

■ ACKNOWLEDGMENT

This work was supported by grants from the National Grand Fundamental Research 973 Program of China (2010CB631301) and the National Natural Science Foundation of China (NSFC-10874007, 20973010, and 21173007).

■ REFERENCES

(1) Novoselov, K. S.; Geim, A. K.; Morozov, S. V.; Jiang, D.; Zhang, Y.; Dubonos, S. V.; Grigonrieva, I. V.; Firsov, A. A. *Science* **2004**, *306*, 666.
(2) Novoselov, K. S.; Jiang, D.; Schedin, F.; Booth, T. J.; Khotkevich, V. V.; Morozov, S. V.; Geim, A. K. *Proc. Natl. Acad. Sci. U.S.A.* **2005**, *102*, 10451.
(3) Bai, J.; Zhong, X.; Jiang, S.; Huang, Y.; Duan, X. *Nat. Nanotechnol.* **2010**, *5*, 190.
(4) Abel, M.; Clair, S.; Ourdjini, O.; Mossoyan, M.; Porte, L. *J. Am. Chem. Soc.* **2011**, *133*, 1203.
(5) Minor, P. C.; Gouterman, M.; Lever, A. B. P. *Inorg. Chem.* **1985**, *24*, 1894.
(6) Martin, P. C.; Gouterman, M.; Pepich, B. V.; Renzoni, G. E.; Schindele, D. C. *Inorg. Chem.* **1991**, *30*, 3305.
(7) Liao, M.-S.; Scheiner, S. *J. Chem. Phys.* **2001**, *114*, 9780.
(8) Peralta, G. A.; Seth, M.; Zhekova, H.; Ziegler, T. *Inorg. Chem.* **2008**, *47*, 4185.
(9) Kroll, T.; Aristov, V. Yu.; Molodtsova, O. V.; Ossipyan, Yu. A.; Vyalikh, D. V.; Buchner, B.; Knupfer, M. *J. Phys. Chem. A* **2009**, *113*, 8917.
(10) Wang, J.; Shi, Y.; Cao, J.; Wu, R. *Appl. Phys. Lett.* **2009**, *94*, No. 122502.
(11) Bhattacharjee, S.; Brena, B.; Banerjee, R.; Wende, H.; Eriksson, O.; Sanyal, B. *Chem. Phys.* **2010**, *377*, 96.
(12) Heutz, S.; Mitra, C.; Wu, W.; Fisher, A. J.; Kerridge, A.; Stoneham, M.; Harker, T. H.; Gardener, J.; Tseng, H.-H.; Jones, T. S.; Renner, C.; Aeppli, G. *Adv. Mater.* **2007**, *19*, 3618.
(13) Chen, X.; Fu, Y.-S.; Ji, S.-H.; Zhang, T.; Cheng, P.; Ma, X.-C.; Zou, X.-L.; Duan, W.-H.; Jia, J.-F.; Xue, Q.-K. *Phys. Rev. Lett.* **2008**, *101*, No. 197208.
(14) Chen, L.; Hu, Z.; Zhao, A.; Wang, B.; Luo, Y.; Yang, J.; Hou, J. G. *Phys. Rev. Lett.* **2007**, *99*, No. 146803.
(15) Zeis, R.; Siegrist, T.; Kloc, Ch. *Appl. Phys. Lett.* **2005**, *86*, No. 022103.
(16) Zhao, A.; Li, Q.; Chen, L.; Xiang, H.; Wang, W.; Pan, S.; Wang, B.; Xiao, X.; Yang, J.; Hou, J. G.; Zhu, Q. *Science* **2005**, *309*, 1542.
(17) Jiang, N.; Zhang, Y. Y.; Liu, Q.; Cheng, Z. H.; Deng, Z. T.; Du, S. X.; Gao, H.-J.; Beck, M. J.; Pantelides, S. T. *Nano Lett.* **2010**, *10*, 1184.
(18) Gao, L.; Ji, W.; Hu, Y. B.; Cheng, Z. H.; Deng, Z. T.; Liu, Q.; Jiang, N.; Lin, X.; Guo, W.; Du, S. X.; Hofer, W. A.; Xie, X. C.; Gao, H.-J. *Phys. Rev. Lett.* **2007**, *99*, No. 106402.
(19) Fu, Y.-S.; Ji, S.-H.; Chen, X.; Ma, X.-C.; Wu, R.; Wang, C.-C.; Duan, W.-H.; Qiu, X.-H.; Sun, B.; Zhang, P.; Jia, J.-F.; Xue, Q.-K. *Phys. Rev. Lett.* **2007**, *99*, No. 256601.
(20) Sun, J. T.; Gao, L.; He, X. B.; Cheng, Z. H.; Deng, Z. T.; Lin, X.; Hu, H.; Du, S. X.; Liu, F.; Gao, H.-J. *Phys. Rev. B* **2011**, *83*, No. 115419.
(21) Dou, W.; Huang, S.; Zhang, R. Q.; Lee, C. S. *J. Chem. Phys.* **2011**, *134*, No. 094705.
(22) Grill, L.; Dyer, M.; Lafferentz, L.; Persson, M.; Peters, M. V.; Hecht, S. *Nat. Nanotechnol.* **2007**, *2*, 687.
(23) Oison, V.; Koudia, M.; Abel, M.; Porte, L. *Phys. Rev. B* **2007**, *75*, No. 035428.
(24) Perdew, J. P.; Burke, K.; Ernzerhof, M. *Phys. Rev. Lett.* **1996**, *77*, 3865.
(25) Kresse, G.; Furthmuller, J. *Phys. Rev. B* **1996**, *54*, 11169.
(26) Anisimov, V. I.; Aryasetiawan, F.; Lichtenstein, A. I. *J. Phys.: Condens. Matter* **1997**, *9*, 767.
(27) Okabayashi, J.; Okabayashi, J.; Rader, O.; Mizokawa, T.; Fujimori, A.; Hayashi, T.; Tanaka, M. *Phys. Rev. B* **1998**, *58*, R4211.

(28) Sato, K.; Bergqvist, L.; Kudrnovský, J.; Dederichs, P. H.; Eriksson, O.; Turek, I.; Sanyal, B.; Bouzerar, G.; Katayama-Yoshida, H.; Dinh, V. A.; Fukushima, T.; Kizaki, H.; Zeller, R. *Rev. Mod. Phys.* **2010**, *82*, 1633.
(29) Sato, K.; Dederichs, P. H.; Katayama-Yoshida, H.; Kudrnovsky, J. *J. Phys.: Condens. Matter* **2004**, *16*, 5491.
(30) Panchmatia, P. M.; Sanyal, B.; Oppeneer, P. M. *Chem. Phys.* **2008**, *343*, 47.
(31) Bernien, M.; Miguel, J.; Weis, C.; Ali, Md. E.; Kurde, J.; Krumme, B.; Panchmatia, P. M.; Sanyal, B.; Piantek, M.; Srivastava, P.; Baberschke, K.; Oppeneer, P. M.; Eriksson, O.; Kuch, W.; Wende, H. *Phys. Rev. Lett.* **2009**, *102*, No. 047202.
(32) Shick, A. B.; Kudrnovsky, J.; Drchal, V. *Phys. Rev. B* **2004**, *69*, No. 125207.
(33) Blöchl, P. E. *Phys. Rev. B* **1994**, *50*, 17953.
(34) Kresse, G.; Joubert, D. *Phys. Rev. B* **1999**, *59*, 1758.
(35) Vosko, S. H.; Wilk, L.; Nusair, M. *Can. J. Phys.* **1980**, *58*, 1200.
(36) Monkhorst, H. J.; Pack, J. D. *Phys. Rev. B* **1976**, *13*, 5188.
(37) Wolska, A.; Lawniczak-Jablonska, K.; Klepka, M.; Walczak, M. S.; Misiuk, A. *Phys. Rev. B* **2007**, *75*, No. 113201.
(38) Zeng, L.; Helgren, E.; Rahimi, M.; Hellman, F.; Islam, R.; Wilkens, B. J.; Culbertson, R. J.; Smith, D. J. *Phys. Rev. B* **2008**, *77*, No. 073306.
(39) *Lange's Handbook of Chemistry*, 15th ed.; Dean, J. A., Ed.; McGraw-Hill: New York, 1999.
(40) Xiang, H.; Yang, J.; Hou, J. G.; Zhu, Q. *J. Am. Chem. Soc.* **2006**, *128*, 2310.
(41) Wu, X.; Zeng, X. C. *J. Am. Chem. Soc.* **2009**, *131*, 14246.
(42) Dietl, T. *Nat. Mater.* **2010**, *9*, 965.
(43) Wang, Q.; Sun, Q.; Jena, P.; Kawazoe, Y. *Phys. Rev. Lett.* **2004**, *93*, No. 155501.
(44) Wang, Q.; Sun, Q.; Jena, P. *Phys. Rev. Lett.* **2005**, *95*, No. 167202.
(45) Dietl, T.; Ohno, H.; Matsukura, F.; Cibert, J.; Ferrand, D. *Science* **2000**, *287*, 1019.
(46) Wang, Q.; Sun, Q.; Jena, P.; Kawazoe, Y. *Phys. Rev. B* **2009**, *79*, No. 115407.